

## **Cluster Beam Deposition of Ultrafine Cobalt and Ruthenium Clusters for Efficient and Stable Oxygen Evolution Reaction**

Junyuan Xu,<sup>†</sup> Shane Murphy,<sup>‡,⊥</sup> Dehua Xiong,<sup>†,§</sup> Rongsheng Cai,<sup>‡,⊥</sup> Xian-Kui Wei,<sup>Δ</sup> Marc Heggen,<sup>Δ</sup> Emanuele Barborini,<sup>¶</sup> Simone Vinati,<sup>¶</sup> Rafal E. Dunin-Borkowski,<sup>Δ</sup> Richard E. Palmer,<sup>⊥,\*</sup> Lifeng Liu<sup>†,\*</sup>

<sup>†</sup> International Iberian Nanotechnology Laboratory (INL), 4715-330 Braga, Portugal

<sup>‡</sup> Nanoscale Physics Research Laboratory, School of Physics and Astronomy, University of Birmingham, Birmingham, B15 2TT, UK

<sup>⊥</sup> College of Engineering, Swansea University, Bay Campus, Fabian Way, Swansea SA1 8EN, UK

<sup>Δ</sup> Ernst Ruska-Centre for Microscopy and Spectroscopy with Electrons and Peter Grünberg Institute, Forschungszentrum Jülich, 52425 Jülich, Germany

<sup>¶</sup> Tethis S.p.A, via Russoli 3, 20143 Milano, Italy

<sup>⊥</sup> Present address: Department of Applied Science, Institute of Technology Tallaght, Dublin 24, Ireland

<sup>§</sup> Present address: State Key Laboratory of Silicate Materials for Architectures, Wuhan University of Technology, Wuhan 430070, P. R. China

\* Corresponding authors. E-mails: [r.e.palmer@swansea.ac.uk](mailto:r.e.palmer@swansea.ac.uk) (R.E. Palmer);

[lifeng.liu@inl.int](mailto:lifeng.liu@inl.int) (L.F. Liu);

## **Experimental details:**

### **Pre-treatment of carbon paper (CP) substrate.**

Prior to CBD of cobalt and ruthenium clusters, the CP substrate (FuelCellStore) with a size of 4 cm × 4 cm was firstly treated in a mixed solution of sulfuric acid and nitric acid (v (98% H<sub>2</sub>SO<sub>4</sub>):v (70% HNO<sub>3</sub>):v (H<sub>2</sub>O) = 1:1:1) at 70 °C for 2 h under rigorous stirring. The as-treated CP substrate was subsequently washed with deionized water and dried at 50 °C in a vacuum oven for 5 h.

### **Deposition of cobalt and ruthenium clusters.**

The Co clusters were prepared using the recently developed Matrix Assembly Cluster Source (MACS).<sup>1,2</sup> Briefly, a solid solution comprising metal atoms and clusters embedded in a condensed noble gas matrix was produced by co-depositing the noble gas and metal onto a cryogenically-cooled support. The matrix was then sputtered with an Ar<sup>+</sup> beam to produce metal nanoclusters, which emerged in a plume from the matrix. The MACS technique is able to generate a cluster beam flux that is at least 2-3 orders of magnitude higher than that produced by conventional mass-filtered cluster beam sources,<sup>3</sup> while retaining the clean (vacuum) environment and ligand-free clusters characteristic of the cluster beam approach. A mass-filtering step is not applied with MACS. Instead, the cluster size is controlled via the metal loading of the matrix, the matrix temperature and the sputtering parameters. Good control over cluster size can be obtained, with coefficients of variation (CoV) in diameter of 10 % and 33 % reported for the deposition of Ag clusters (in the 1.2 nm – 3.4 nm diameter range) in transmission mode<sup>1</sup> and reflection mode,<sup>3</sup> respectively. The latter value is comparable to what was observed for the Co clusters in the present study (31 % for 3.2 nm clusters and 44 % for 1.8 nm clusters), which were also deposited in reflection mode. The instrument employed in the present work is described in Ref. [2]. The matrix was produced by depositing Co at a rate

of  $0.42 \text{ nm min}^{-1}$  by electron-beam evaporation (SPECS EBE-1) of a 99.95 % pure Co rod for 120 min onto an oxygen-free copper support, while simultaneously backfilling the vacuum chamber with Ar gas to a pressure of  $4 \times 10^{-6}$  mbar using a leak valve. This resulted in a metal loading inside the matrix of 6.1 % by number of atoms. The Co deposition flux was monitored using a quartz crystal microbalance, while the temperature of the matrix was monitored via a rhodium-iron temperature sensor (Lakeshore RF-100) inserted into the matrix support. The temperature of the matrix remained below 25 K during the deposition process. After deposition, a linear translator was used to move the matrix into a second chamber, which housed a rotatable sample carousel designed to hold multiple substrates (i.e. 21 glass microscope slides). The CP substrates were mounted on this sample carousel. Nanoclusters were deposited by ion beam sputtering of the matrix with 1.5 keV  $\text{Ar}^+$  ions at a sputter current of 30  $\mu\text{A}$  for 40 min. The cluster beam produced allows a relatively large substrate area to be coated without the need to raster the beam. Uniform deposition with less than  $\pm 20$  % variation in mean nanocluster coverage, has been observed over the area of a standard glass microscope slide (i.e.  $25 \text{ mm} \times 75 \text{ mm}$ ).

The Ru clusters were deposited on CP substrates by a Pulsed Microplasma Cluster Source (PMCS).<sup>4-6</sup> This method allows the direct deposition at room temperature of a cluster-assembled, uniform, and nanoporous catalyst layer onto the substrates of interest, by exposing them to the cluster beam. Coverage uniformity is ensured by the rastering of the substrates in front of the cluster beam. The rastered area typically includes a quartz microbalance thickness monitor that provides real-time information on deposited thickness. PMCS principle of operation exploits the confinement of a high-voltage, high-current pulsed electric discharge into an Ar jet, thanks to gas-dynamic phenomena. The pulsed electrical discharge vaporizes Ruthenium atoms from a 2-mm diameter metallic rod (Testbourne Ltd, 99.95% purity). The thermalization and subsequent aggregation of Ruthenium atoms in clusters/nanoparticles,

occur in pure Ar atmosphere (Linde Gas, 6.0 purity). Finally, the Ar-nanoparticles mixture undergoes a supersonic expansion through the PMCS nozzle, driven by the pressure drop towards a vacuum chamber that generates the cluster beam. Being of the order of the tenth of eV, the kinetic energy per atom of the clusters in the beam is sufficiently low to prevent the fragmentation of the clusters and basically any phenomenon of surface diffusion, ensuring the growth of the film to occur according to the so-called ballistic model,<sup>7</sup> which is responsible of the layer porosity at the nanometric scales and related large specific surface, typically of the order of  $100 \text{ m}^2 \text{ g}^{-1}$ . Once the deposition is completed, the coated substrates are unloaded from the deposition chamber, and the exposure to air causes the surface oxidation of metallic Ruthenium clusters.

### **Materials characterization.**

Co clusters were simultaneously deposited onto TEM grids coated with amorphous carbon for characterization in a 200 keV (JEOL 2100F) STEM with a spherical aberration corrector (CEOS) and a resolution of 0.1 nm. HAADF images were acquired with inner and outer detector angles of 62 mrad and 164 mrad, respectively (camera length of 10 cm), and a probe convergence angle of 20 mrad. Particle size distributions (PSD) were obtained using threshold analysis using Fiji.<sup>8</sup> Because of the large difference in HAADF intensity between the large and small clusters, it was impossible to set the threshold level low enough to accurately measure the small clusters without ‘washing out’ the larger clusters so that they appeared much larger. Also, the number of small clusters per unit area far exceeded that of the larger clusters, with a sample size of ~250 large clusters and ~13000 small clusters obtained from the recorded STEM images. This meant that a second peak due to the larger clusters was not noticeable in the overall PSD. Consequently, separate distributions were measured for each cluster type, with lower magnification ( $10^6 \times$ ) images used to measure the larger clusters, and higher

magnification ( $2.10^6 \times - 4.10^6 \times$ ) images to measure the small clusters. The Feret diameter was recorded for the PSD of the smaller clusters, which was also cropped on the left-hand side to remove spurious noise from the analysis.

Ru clusters were also directly deposited on a carbon-coated TEM grid. The HAADF and EDX examinations were carried out on an FEI Titan 80-200 Chemi-STEM microscope (operated at 200 kV) equipped with bright-field/dark-field STEM detectors and a Super-X dispersive X-ray spectrometer for compositional analysis.

### **Electrocatalytic tests.**

All electrocatalytic tests were carried out in a three-electrode configuration at room temperature using a Biologic VMP-3 potentiostat/galvanostat. The CP supported nanoclusters (area of deposition:  $1 \times 1 \text{ cm}^2$ ; area free of deposition for electrical connection:  $0.5 \times 1 \text{ cm}^2$ ; catalyst loading: 0.075 and  $0.20 \text{ mg cm}^{-2}$  for MACS-Co and PMCS-Ru), a Pt wire and a saturated calomel electrode (SCE) were utilized as working, counter, and reference electrodes, respectively. The SCE reference was calibrated prior to each measurement in Ar/H<sub>2</sub>-saturated 0.5 M H<sub>2</sub>SO<sub>4</sub> solution using a clean Pt wire as the working electrode. 1.0 M KOH was used as electrolyte. Unless otherwise stated, all potentials are reported versus reversible hydrogen electrode (RHE) by converting the measured potentials according to the following equation:

$$E_{\text{RHE}} = E_{\text{SCE}} + 0.059 \times \text{pH} + 0.241 \quad (\text{S1})$$

The commercial Ru/C (20 wt % Ru, product code: 3151601) and RuO<sub>2</sub> (product code: A10816) catalysts were purchased from FuelCellStore and Alfa Aesar, respectively. To prepare a catalyst ink, 5 mg of catalyst powders was firstly dispersed into 1 mL of ethanol containing 50  $\mu\text{L}$  of Nafion® solution, and the solution was ultrasonicated for 60 min. For Ru/C catalysts, 100  $\mu\text{L}$  of catalyst ink were loaded on a CP substrate with an exposed area of  $1 \times 1 \text{ cm}^2$  defined by non-conductive epoxy resin, leading to a loading density of  $0.5 \text{ mg cm}^{-2}$  (Ru loading: 0.1

mg cm<sup>-2</sup>); whereas for RuO<sub>2</sub> catalysts, 20 μL of catalyst ink were loaded on a similar CP substrate, resulting in a loading density of *ca.* 0.1 mg cm<sup>-2</sup>.

All CP working electrodes have a size of 1 cm × 1.5 cm with a defined area of 1 × 1 cm<sup>2</sup> where the catalyst was loaded and exposed to the electrolyte, and an electrode holder was connected with the rest part of the CP substrate free of catalysts. Cyclic voltammetry (CV) was performed at a scan rate of 5 mV s<sup>-1</sup> in the potential range of 1.0 to 1.8 V *vs* RHE. An *iR*-correction (85%) was made to compensate for the voltage drop between the reference and working electrodes, which was measured by a single-point high-frequency (100 kHz) impedance measurement. The obtained compensation resistance values were 1.67, 1.13, 1.71 and 1.07 Ω for commercial RuO<sub>2</sub>, Ru/C, PMCS-Ru and MACS-Co, respectively. Impedance spectroscopy measurements were carried out at 1.50 V *vs* RHE in the frequency range of 10<sup>5</sup> to 0.01 Hz with a 10 mV sinusoidal perturbation. The catalytic stability was assessed using chronopotentiometry at a constant current density of 10 mA cm<sup>-2</sup>.

### **Calculation of TOF.**

The TOF values of all the catalysts were calculated through the following equation:

$$\text{TOF (s}^{-1}\text{)} = (j \times A) / (4 \times F \times n) \quad (\text{S2})$$

where  $j$  (A cm<sup>-2</sup>) is the current density at a given overpotential,  $A = 1.0$  cm<sup>2</sup> is the geometric surface area of the electrode,  $F = 96500$  C mol<sup>-1</sup> stands for the Faraday constant,  $n$  (mol) is mole number of metallic catalysts loaded on the CP substrate. All metal cations in the catalyst were assumed to be catalytically active, so the calculated values represent the lower limits of TOF.

### **Determination of ECSA.**

The electrochemically accessible surface area (ECSA) can be obtained as follows:

$$ECSA = C_{dl} / C_{dl0} \quad (S3)$$

where  $C_{dl}$  is the double-layer capacitance of the catalysts measured by cyclic voltammetry in the non-Faradaic potential region (**Figure S4**), while  $C_{dl0}$  represents the double-layer capacitance of a model Co or Ru catalyst on a unit surface area, which is usually assumed to be  $0.04 \text{ mF cm}_{\text{geo}}^{-2}$ , according to previous reports.<sup>9,10</sup> The specific activity of catalysts can then be obtained through dividing the catalytic current by the ECSA.

## Supporting Figures

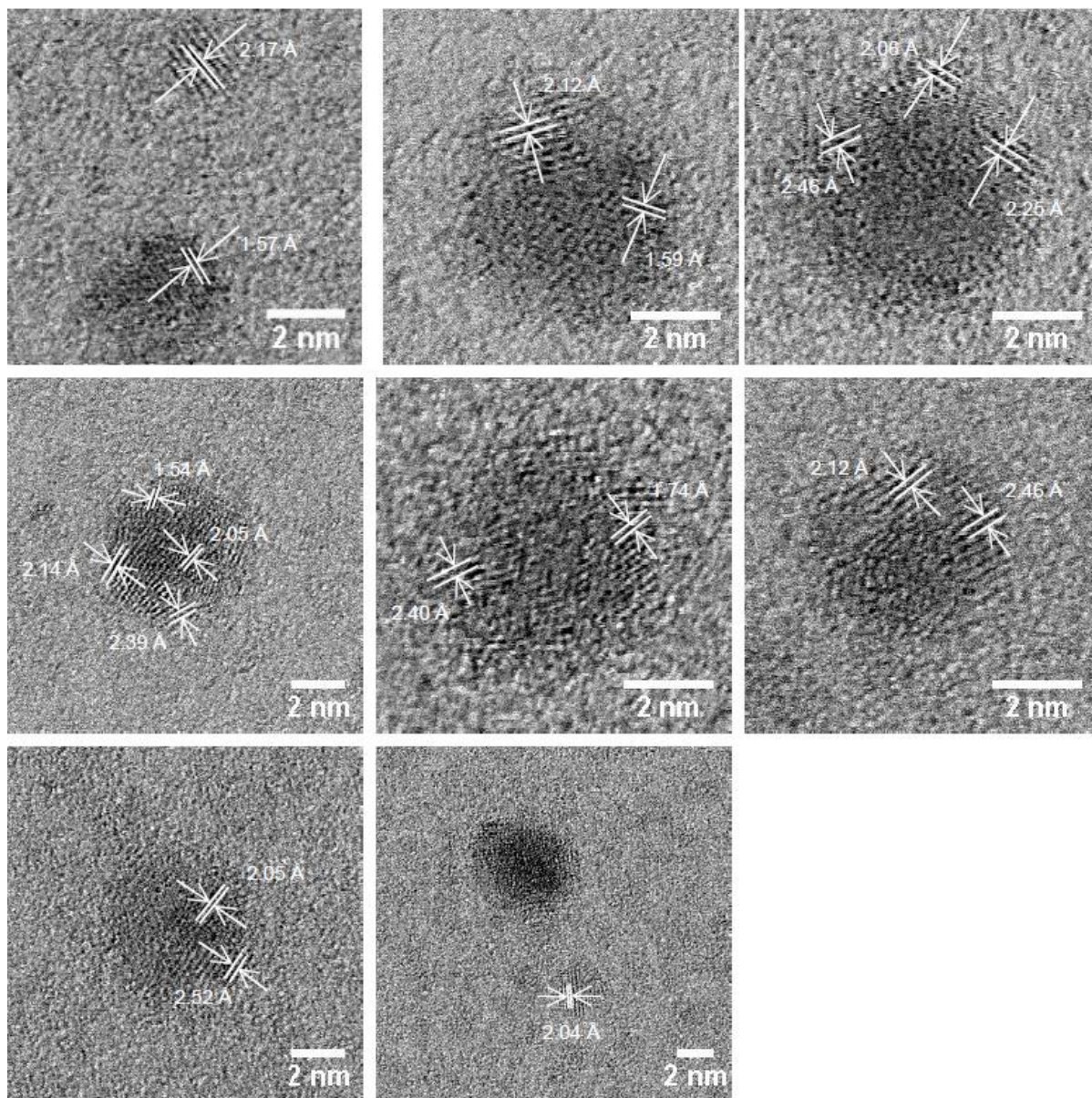


**Figure S1.** Representative HRSTEM images showing the oxidation of Co clusters upon exposure in air. The distances of  $\sim 2.15$  Å and  $\sim 2.46$  Å correspond to the interlayer distance between the (200) and (111) planes of CoO, respectively. The distance of  $\sim 1.54$  Å may correspond to the (220) plane of CoO. The distance of  $\sim 2.05$  Å corresponds to the interlayer separation between Co (002) planes.

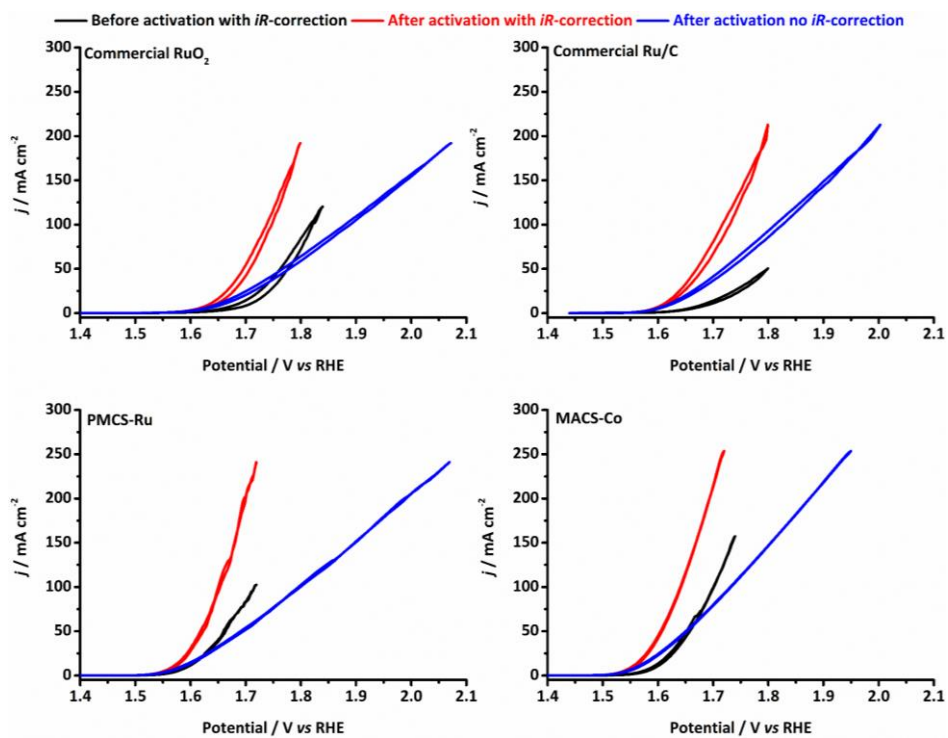


**Figure S2.** The CV curves of all the catalysts before and after pre-activation.

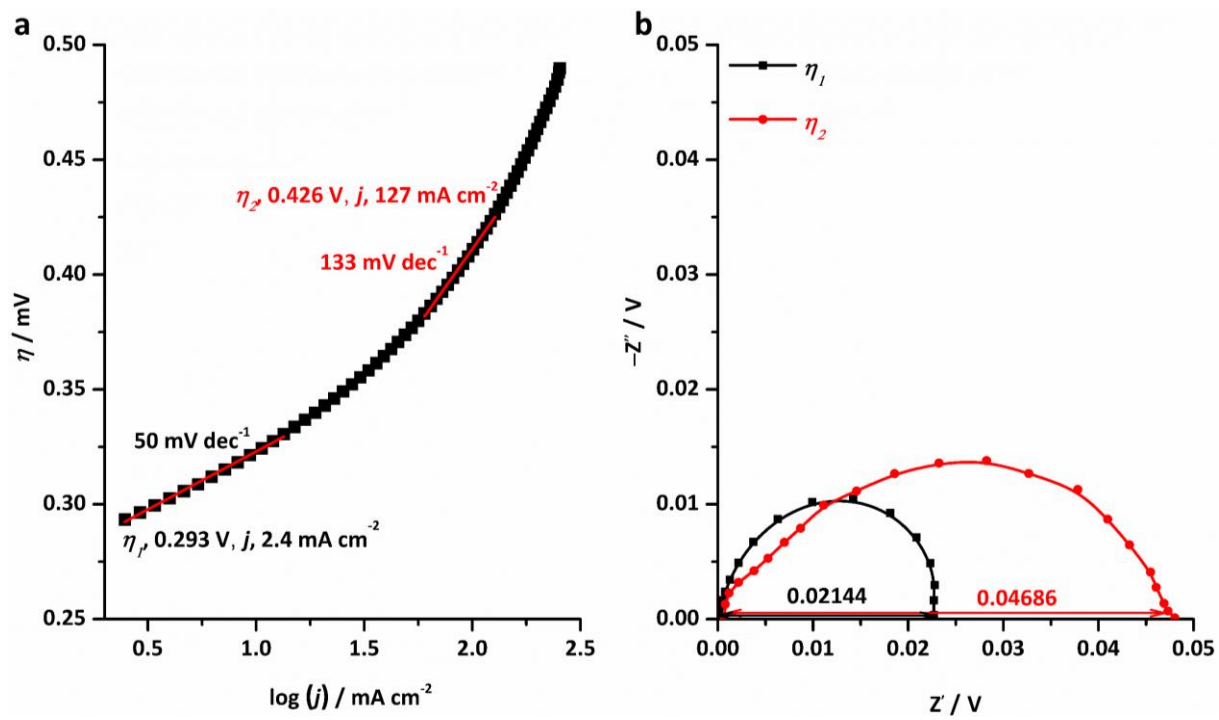


**Figure S3.** (a) Tafel analysis and (b) Tafel impedance spectrum of MACS-Co.

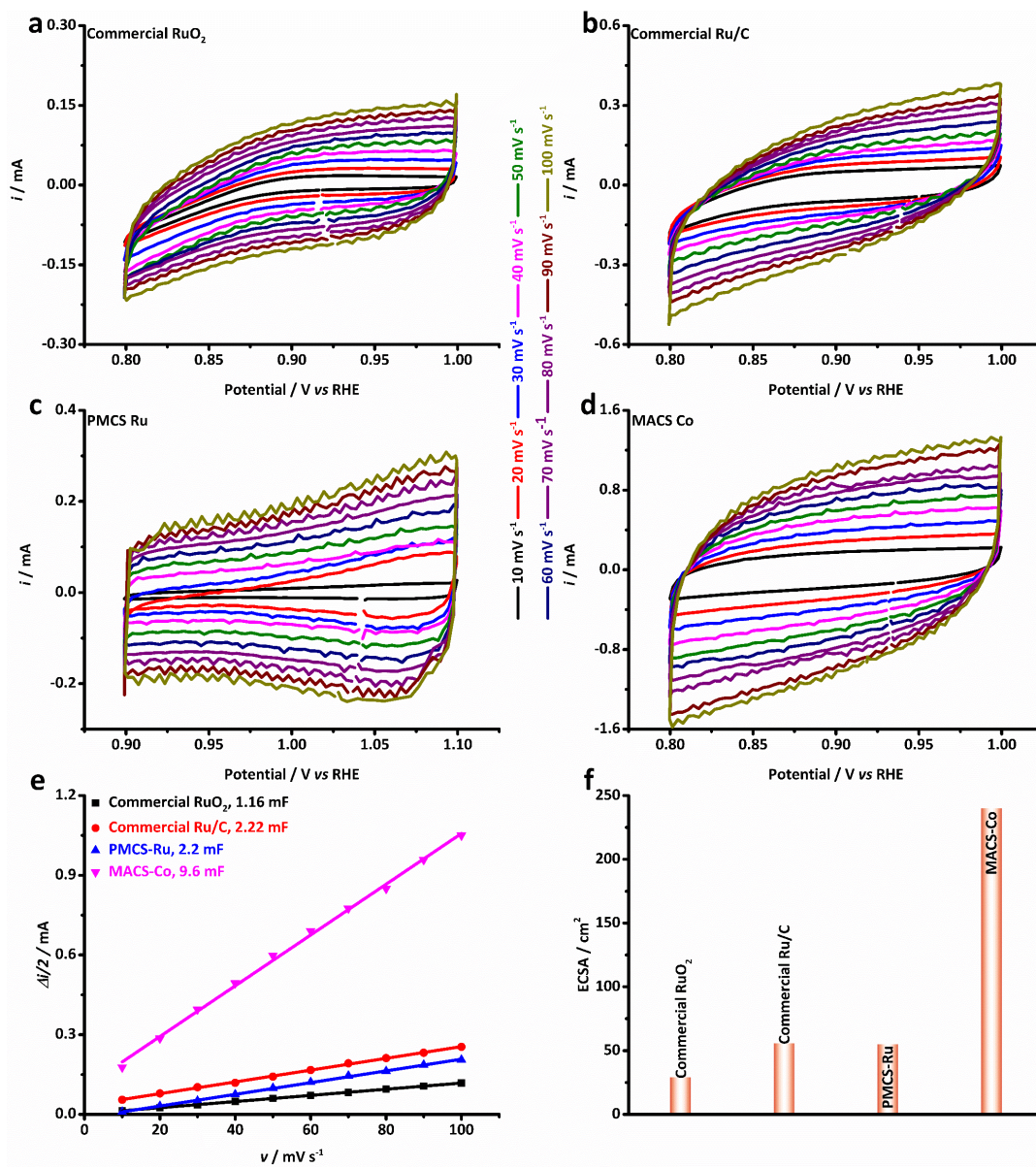


**Figure S4.** (a-d) CV curves of all the catalysts recorded at different scan rates of 10, 20, 30, 40, 50, 60, 70, 80, 90 and 100  $\text{mV s}^{-1}$ . (e) Double-layer capacitance and (f) ECSA of all the catalysts.

## Supporting Tables

**Table S1.** Comparison of the OER performance of Co clusters with that of other non-precious OER catalysts reported in the literature.

Catalysts	Substrate	Loading (mg cm <sup>-2</sup> )	$\eta_{10}$ (mV) <sup>a</sup>	Tafel slope (mV dec <sup>-1</sup> )	$TOF_{300}$ (s <sup>-1</sup> ) <sup>b</sup>	References
<b>MACS-Co cluster</b>	<b>CP</b>	<b>0.075</b>	<b>320</b>	<b>50</b>	<b>0.01</b>	<b>This work</b>
Zn <sub>x</sub> Co <sub>3-x</sub> O <sub>4</sub> Nanoarray	Ti foil	1.0	320	51	ca. 0.0008	11
CoP film	Cu foil	/	345	47	/	12
CoP nanorod	GCE <sup>c</sup>	0.71	320	71	ca. 0.002	13
Ni <sub>x</sub> Co <sub>3-x</sub> O <sub>4</sub> nanowire	Ni foam	0.70	335	75	ca. 0.0007	14
CP/CTs/Co-S sheet	CP	0.32	306	72	0.016	15
Fe <sub>3</sub> O <sub>4</sub> @Co <sub>9</sub> S <sub>8</sub> /rGo NP	GCE	0.25	320	54.5	ca. 0.0045	16
CoS-Co(OH) <sub>2</sub> @aMoS <sub>2+x</sub> /NF	Ni foam	0.20	380	68	/	17
CoMnP NP	GCE	0.284	330	61	ca. 0.004	18
O-CoP/GO NP	GCE	0.28	280	75	ca. 0.01	19
Ni <sub>0.75</sub> Fe <sub>0.25</sub> -LDH nanosheet	GCE	0.143	318	50	ca. 0.01	20
FeO <sub>x</sub> /CFC nanosheet	CP	/	359	93	/	21
Ni <sub>3</sub> C/C nanoparticle	CP	0.285	ca. 310	46	ca. 0.009	22
Co-C <sub>3</sub> N <sub>4</sub> /CNT NP	RDE <sup>d</sup>	0.41	380	68.4	/	23
NiCoP/C NP	RDE	0.13	330	96	/	24
CS-Co/C NP	GCE	0.20	290	70	0.015	25
Fe <sub>1.1</sub> Mn <sub>0.9</sub> P nanorod	GCE	0.284	440	39	/	26

<sup>a</sup> The overpotential at the current density of 10 mA cm<sup>-2</sup>.  
<sup>b</sup> The TOF value at the overpotential of 300 mV.  
<sup>c</sup> GCE (Glassy carbon electrode).  
<sup>d</sup> RDE (Rotating disk electrode).

**Table S2.** Fitting parameters for the Nyquist plots of all the catalysts.

<b>Catalysts</b>	<b>R<sub>s</sub></b> <b>(<math>\Omega</math>)</b>	<b>R<sub>1</sub></b> <b>(<math>\Omega</math>)</b>	<b>CPE<sub>1</sub></b> <b>(<math>\mu</math>F)</b>	<b>R<sub>ct</sub></b> <b>(<math>\Omega</math>)</b>	<b>CPE<sub>2</sub></b> <b>(<math>\mu</math>F)</b>
Commercial RuO <sub>2</sub>	1.7	0.42	286	186	2200
Commercial Ru/C	1.15	0.38	163	156	1563
PMCS-Ru cluster	1.7	0.29	66	37	460
MACS-Co cluster	1.10	0.25	41	32	329

## References

- (1) Palmer, R. E.; Cao, L.; Yin, F. Proof of Principle of A New Type of Cluster Beam Source with Potential for Scale-Up. *Rev. Sci. Instrum.* **2016**, *87*, 046103.
- (2) Cai, R. S.; Jian, N.; Murphy, S.; Bauer, K.; Palmer, R. E. A New Method to Prepare Colloids of Size-Controlled Clusters From A Matrix Assembly Cluster Source. *APL Mater.* **2017**, *5*, 053405.
- (3) Ellis, P. R.; Brown, C. M.; Bishop, P. T.; Yin, J.; Cooke, K.; Terry, W. D.; Liu, J.; Yin, F., Palmer, R. E. The Cluster Beam Route to Model Catalysts and Beyond. *Faraday Discuss.* **2016**, *188*, 39-56.
- (4) Milani, P; Iannotta, S. Cluster Beam Synthesis of Nanostructured Materials, Springer, Berlin, 1999.
- (5) Barborini, E.; Piseri, P.; Milani, P. A Pulsed Microplasma Source of High Intensity Supersonic Carbon Cluster Beams, *J. Phys. D: Appl. Phys.* **1999**, *32*, L105-L109.
- (6) Wegner, K.; Piseri, P.; Vahedi Tafreshi, H.; Milani, P. Cluster Beam Deposition: A Tool for Nanoscale Science and Technology. *J. Phys. D: Appl. Phys.* **2006**, *39*, R439-R459.
- (7) Barabasi, A. L.; Stanley, H. E. Fractal Concepts in Surface Growth, Cambridge University Press, Cambridge, England, 1995.
- (8) Schindelin, J.; Arganda-Carreras, I.; Frise, E. Fiji: an open-source platform for biological-image analysis. *Nat. methods* **2012**, *9*, 676-682.
- (9) McCrory, C. C. L.; Jung, S. H.; Ferrer, I. M.; Chatman, S. M.; Peters, J. C.; Jaramillo, T. F. Benchmarking Hydrogen Evolving Reaction and Oxygen Evolving Reaction Electrocatalysts for Solar Water Splitting Devices. *J. Am. Chem. Soc.* **2015**, *137*, 4347-4357.

- (10) Li, K.; Li, Y.; Wang, Y. M.; Ge, J. J.; Liu, C. P.; Xing, W. Enhanced electrocatalytic performance for the hydrogen evolution reaction through surface enrichment of platinum nanoclusters alloying with ruthenium *in situ* embedded in carbon. *Energy Environ. Sci.* **2018**, 10.1039/C8EE00402A.
- (11) Liu, X. J.; Chang, Z.; Luo, L.; Xu, T. H.; Lei, X. D.; Liu, J. F.; Sun, X. M. Hierarchical  $Zn_xCo_{3-x}O_4$  Nanoarrays with High Activity for Electrocatalytic Oxygen Evolution. *Chem. Mater.* **2014**, 26, 1889-1895.
- (12) Jiang, N.; You, B.; Sheng, M. L.; Sun, Y. J. Electrodeposited Cobalt-Phosphorous-Derived Films as Competent Bifunctional Catalysts for Overall Water Splitting. *Angew. Chem. Int. Ed.* **2015**, 54, 6251-6254.
- (13) Chang, J. F.; Xiao, Y.; Xiao, M. L. Ge, J. J.; Liu, C. P.; Xing, W. Surface Oxidized Cobalt-Phosphide Nanorods As an Advanced Oxygen Evolution Catalyst in Alkaline Solution. *ACS Catal.* **2015**, 5, 6874-6878.
- (14) Yan, X. D.; Li, K. X.; Lyu, L.; Song, F.; He, J.; Niu, D. M.; Liu, L.; Hu, X. L.; Chen, X. B. From Water Oxidation to Reduction: Transformation from  $Ni_xCo_{3-x}O_4$  Nanowires to NiCo/NiCoO<sub>x</sub> Heterostructures. *ACS Appl. Mater. Interfaces* **2016**, 8, 3208-3214.
- (15) Wang, J.; Zhong, H. X.; Wang, Z. L.; Meng, F. L.; Zhang, X. B. Integrated Three-Dimensional Carbon Paper/Carbon Tubes/Cobalt-Sulfide Sheets as an Efficient Electrode for Overall Water Splitting. *ACS Nano* **2016**, 10, 2342-2348.
- (16) Yang, J.; Zhu, G. X.; Liu, Y. J.; Xia, J. X.; Ji, Z. Y.; Shen, X. P.; Wu, S. K. Fe<sub>3</sub>O<sub>4</sub>-Decorated Co<sub>9</sub>S<sub>8</sub> Nanoparticles In Situ Grown on Reduced Graphene Oxide: A New and Efficient Electrocatalyst for Oxygen Evolution Reaction. *Adv. Funct. Mater.* **2016**, 26, 4712-4721.

- (17) Yoon, T. S.; Kim, K. S. One-Step Synthesis of CoS-Doped  $\beta$ -Co(OH)<sub>2</sub>@Amorphous MoS<sub>2+x</sub> Hybrid Catalyst Grown on Nickel Foam for High-Performance Electrochemical Overall Water Splitting *Adv. Funct. Mater.* **2016**, *26*, 7386-7393.
- (18) Li, D.; Baydoun, H.; Verani, C. N.; Brock, S. Efficient Water Oxidation Using CoMnP Nanoparticles. *J. Am. Chem. Soc.* **2016**, *138*, 4006-4009.
- (19) Zhang, G.; Wang, G. C.; Liu, Y.; Liu, H. J.; Qu J. H.; Li, J. H. Highly Active and Stable Catalysts of Phytic Acid-Derivative Transition Metal Phosphides for Full Water Splitting. *J. Am. Chem. Soc.* **2016**, *138*, 14686-14693.
- (20) Fan, K.; Chen, H.; Ji, Y. F.; Huang, H.; Claesson, P. M.; Daniel, Q.; Philippe, B.; Rensmo, H.; Li, F. S.; Luo, Y.; Sun, L. C. Nickel-Vanadium Monolayer Double Hydroxide for Efficient Electrochemical Water Oxidation. *Nat. Commun.* **2016**, *7*, 11981.
- (21) Yan, F.; Zhu, C. L.; Wang, S.; Zhao, Y.; Zhang, X. T.; Li, C. Y.; Chen, Y. J. Electrochemically activated-iron oxide nanosheet arrays on carbon fiber cloth as a three-dimensional self-supported electrode for efficient water oxidation. *J. Mater. Chem. A* **2016**, *4*, 6048-6055.
- (22) Xu, K.; Ding, H.; Lv, H. F.; Chen, P. Z.; Lu, X. L.; Cheng, H.; Zhou, T. P.; Liu, S.; Wu, X. J.; Wu, C. J.; Xie, Y. Dual Electrical-Behavior Regulation on Electrocatalysts Realizing Enhanced Electrochemical Water Oxidation. *Adv. Mater.* **2016**, *28*, 3326.
- (23) Zheng, Y.; Jiao, Y.; Zhu, Y. H.; Cai, Q. R.; Vasileff, A.; Li, L. H.; Han, Y.; Chen, Y.; Qiao, S. Z. Molecule-Level g-C<sub>3</sub>N<sub>4</sub> Coordinated Transition Metals as a New Class of Electrocatalysts for Oxygen Electrode Reactions *J. Am. Chem. Soc.* **2017**, *139*, 3336-3339.

- (24) He, P. L.; Yu, X. Y.; Lou, X. W. Carbon-Incorporated Nickel–Cobalt Mixed Metal Phosphide Nanoboxes with Enhanced Electrocatalytic Activity for Oxygen Evolution. *Angew. Chem. Int. Ed.* **2017**, *56*, 3897-3900.
- (25) Zhao, J. J.; Quan, X.; Chen, S.; Liu, Y. M.; Yu, H. T. Cobalt Nanoparticles Encapsulated in Porous Carbons Derived from Core–Shell ZIF67@ZIF8 as Efficient Electrocatalysts for Oxygen Evolution Reaction. *ACS Appl. Mater. Interfaces* **2017**, *9*, 28685-28694.
- (26) Li, D.; Baydoun, H.; Kulikowski, B.; Brock, S. L. Boosting Catalytic Performance of Iron Phosphide Nanorods for the Oxygen Evolution Reaction by Incorporation of Manganese. *Chem. Mater.* **2017**, *29*, 3048-3054.